Title

Probing the Substrate Specificity and Protein-Protein Interactions of the E. coli Fatty Acid Dehydratase, FabA

Journal

Cell Chemical Biology, 22(11)

ISSN

2451-9456

Authors

Finzel, Kara
Nguyen, Chi
Jackson, David R
et al.

Publication Date

2015-11-01

DOI

10.1016/j.chembiol.2015.09.009

Peer reviewed

HHS Public Access

Author manuscript

Chem Biol. Author manuscript; available in PMC 2016 November 19.

Published in final edited form as:

Chem Biol. 2015 November 19; 22(11): 1453–1460. doi:10.1016/j.chembiol.2015.09.009.

Probing the Substrate Specificity and Protein-Protein Interactions of the *E. coli* Fatty Acid Dehydratase, FabA

Kara Finzel[1,+], **Chi Nguyen**[2,+], **David R. Jackson**[2], **Aarushi Gupta**[1], **Shiou-Chuan Tsai**[2,*], and **Michael D. Burkart**[1,*]

[1]Department of Chemistry and Biochemistry, University of California, San Diego, La Jolla, California 92093-0358 (USA)

[2]Departments of Molecular Biology and Biochemistry, Chemistry and Pharmaceutical Sciences, University of California, Irvine, Irvine, California 92697-1450 (USA)

Summary

Microbial fatty acid biosynthetic enzymes are important targets for areas as diverse as antibiotic development to biofuel production. Elucidating the molecular basis of chain length control during fatty acid biosynthesis is crucial for the understanding of regulatory processes of this fundamental metabolic pathway. In *Escherichia coli*, the acyl carrier protein (AcpP) plays a central role by sequestering and shuttling the growing acyl chain between fatty acid biosynthetic enzymes. FabA, a β-hydroxylacyl-AcpP dehydratase, is an important enzyme in controlling fatty acid chain length and saturation levels. FabA-AcpP interactions are transient in nature and thus difficult to visualize. In this study, four mechanistic crosslinking probes mimicking varying acyl chain lengths were synthesized to systematically probe for modified chain length specificity of fourteen FabA mutants. These studies provide evidence for the AcpP interacting “positive patch,” FabA mutations that altered substrate specificity, and the roles that the FabA “gating residues” play in chain-length selection.

Introduction

Escherichia coli provides the paradigm for the dissociated type II fatty acid synthase (FAS II) pathway, typically found in bacteria and plants. In FAS II, a discrete protein catalyzes each step, and iterative enzymatic reactions for chain elongations and modification biosynthesize the fatty acid products. Central to this process is the acyl carrier protein (AcpP

*Designates corresponding authors. mburkart@ucsd.edu, http://burkartlab.ucsd.edu, sctsai@ucsd.edu, http://www.tsailabuci.com/.
+These authors contributed equally to this work.

Author contributions

K.F. designed, synthesized and characterized probes **DH6, DH8, DH10**, and **DH10X** and performed *in vivo* studies. C.N. proposed the project, performed site-directed mutagenesis, protein expression and purification, chemo-enzymatic loading of AcpP, and enzymatic assays. D.J. performed chemoenzymatic loading of AcpP, mass spectrometry of AcpP loading and FabA crosslinking, and circular dichroism experiments. A.G. aided in the synthesis and characterization of probes **DH6, DH8, DH10**, and **DH10X**. K.F. and C.N wrote and formatted the paper. D.J., S.T., and M.B. aided in writing and editing the paper.

in *E. coli*), a small acidic protein that is responsible for sequestering and shuttling fatty acid intermediates between the dissociated fatty acid biosynthetic enzymes (Cronan, 2014). Specific interactions between AcpP and its partner proteins signal AcpP to present the growing chain from its interior hydrophobic cavity to the partnered protein for chemical modification (Zhang, 2003; White, 2005; Nguyen, 2014; Masoudi, 2014). How such an intricately choreographed process is accomplished is not fully understood.

Fundamental understanding of the processes involved in fatty acid biosynthesis has important implications for next-generation biofuels and anti-microbial therapeutics. The need for renewable energy sources and novel antibiotics, due to the rise in highly resistant strains of pathogenic bacteria, has prompted vigorous effort to investigate the mechanisms that control fatty acid chain length production and pathway processivity in the *E. coli* FAS II (Janssen, 2013; Lee, 2013; Torella, 2013). In bacteria, fatty acid chain length control occurs during two enzymatic steps: the decarboxylative claisen condensation forming β-ketoacyl-AcpP by three ketosynthases (FabH, FabB, and FabF) and the dehydration of β-hydroxyacyl-AcpP by two dehydratases (FabA and FabZ) (Magnuson, 1993). However, fundamental information about how these enzymes selectively interact with specific acyl chain lengths sequestered by AcpP and control fatty acid chain length production remains to be understood. This lack of knowledge has hindered the application of FAS II for the engineering of next-generation biofuels and antibiotics development.

In *E. coli*, both FabA and FabZ catalyze the dehydration of β-hydroxyacyl-AcpP. FabA additionally catalyzes the isomerization of *trans*-α-decenoyl-AcpP into *cis*-β-decenoyl-AcpP, the first reaction towards the biosynthesis of unsaturated fatty acids in *E. coli* (Feng 2009). FabA most efficiently dehydrates intermediate chain length acyl-AcpPs, between 8 and 12 carbons, with the highest preference for a ten-carbon acyl chain (Heath, 1996). Correspondingly, FabZ has demonstrated preference for the dehydration of short and long-chain acyl-AcpPs, between 4 and 6 carbons, and 14+ carbon chain lengths (Heath, 1996). Comparative analysis of FabA from *E. coli* (PDB codes 1MKA and 1MKB) and FabZ from *Pseudomonas aeruginosa* (PDB code IU1Z) reveals that both enzymes contain similar extended substrate binding tunnels that can accommodate up to 12 carbon chain lengths (Leesong, 1996; Kimber, 2004). Therefore, it is not known how these two classes of dehydratases achieve such divergent substrate specificities.

Recent advances in the understanding of FabA activity were made with the crystal structure of the AcpP=FabA complex using mechanistic-based crosslinking, providing the first visualization of AcpP in functional association with a FabA (Fig. 1) (Nguyen, 2014). Prior to this structure, the transient nature of the interactions between AcpP and partner proteins has posed major challenges in structural and biochemical characterization of FAS II complexes. To better understand the significance of substrate binding and AcpP interaction for FabA activity, we performed structural alignments between three FabA crystal structures: the *apo*-FabA, FabA with the 3-decynoyl-*N*-acetylcysteamine (SNAC) inhibitor (*holo*-FabA) and the AcpP=FabA complex (Fig. S5b)(Leesong, 1996; Nguyen, 2014). Although the three FabA structures are highly similar along their Cα backbones (with RMSD values less than 0.25 A (Table S1)), highlighting important common features between the three FabA structures, the results from these structural comparisons also

revealed structural rearrangements that are important for substrate binding and AcpP interaction.

Comparative analysis of the three FabA structures suggests that the FabA-substrate and FabA-AcpP interactions may be dependent on three defined FabA regions: (1) FabA surface residues that interact with AcpP, (2) “gating residues” at the entrance of the catalytic tunnel, and (3) the substrate-binding tunnel (Fig. 1). To investigate how these regions influence FabA activity, we performed structure-based site-directed mutagenesis at these three defined regions.

In order to explore the activity of the FabA mutants, an active site specific mechanism-based crosslinking assay was employed (Fig. 2 and S1). Mechanism-based crosslinking leads to stable AcpP=FabA complex formation, providing an ideal assay to directly assess the residues guiding FabA substrate specificity and AcpP interaction. FabA-specific mechanistic crosslinking is accomplished by the attachment of a reactive warhead on to pantetheine and chemoenzymatic loading of the pantetheine derivative onto the active site S36 of AcpP (Fig. S1). In this study, the crosslinking probe terminus contains a sulfonyl-3-alkyne reactive warhead, which non-reversibly reacts with the active site H70 of FabA. This produces a stable AcpP=FabA crosslinked complex covalently linked by the AcpP and FabA active sites (Fig. 2a and S1) (Ishikawa, 2013). In this study, quantification of the crosslinking yields between FabA and AcpP *via* gel shift assay and protein mass spectrometry provides a method to directly assess FabA activity and FabA-AcpP interaction (Fig. 2b–c and S3). In order to probe for altered substrate specificities of the FabA mutants, we synthesized four different mechanistic crosslinking probes bearing varying acyl chain lengths to mimic different fatty acid intermediates (Fig. 3). The results from this study reveal the importance of the FabA “positive patch” in AcpP interactions, substrate pocket residues that drive specific acyl chain length dehydration, and the “gating residues” in the initial acyl chain length selection.

Results and Discussion

Probe Synthesis

The original mechanistic crosslinking probe, DH10, was designed to capture AcpP in functional association with the 3-hydroxyacyl-AcpP dehydratase, FabA (Fig. 2, 3 and S1) (Ishikawa, 2013). This was accomplished by leveraging *E. coli* CoA biosynthetic enzymes, pantothenate kinase (PanK), phosphopantetheine adenylyltransferase (PPAT), and dephosphocoenzyme A kinase (DPCK), to convert the pantetheine derivative into a CoA analog. A promiscuous phosphopantetheinyl transferase (PPTase) then loads the CoA analog onto the conserved active site S36 residue of *apo*-AcpP (Fig. S2) (Worthington, 2006).

Probe **DH10** was synthesized from the convergent assembly of commercially available 2-nonyn-1-ol, 3-chloropropylamine and *p*-methoxybenzyl-protected pantothenic acid (synthetic methods provided in the SI, Fig. S2). This allowed for the efficient modification of the alkyne starting material used in order to synthesize crosslinking analogues of varying lengths. Probe **DH10** mimics a 10 carbon acyl chain, the preferred substrate length of *E. coli* FabA (Heath, 1996). To probe for the activity of FabA with varying acyl chain lengths, we

synthesized three new mechanistic crosslinkers that mimic native fatty acid intermediates. Probes **DH6** and **DH8** represent the 6 and 8 carbon acyl chain intermediates, respectively. Probe **DH10X** represents a 10 carbon acyl chain, but with an extended six carbon linker embedded in the phosphopantetheine (PPT) portion. Probe **DH10X** was synthesized to explore the effects of altering PPT arm length on FabA activity (Fig 3 and S2). The loading of probes **DH6**, **DH8**, **DH10**, and **DH10X** onto *apo*-AcpP was monitored using matrix-assisted laser desorption/ionization time of flight mass spectrometry (MALDI-TOF MS) (Fig. S3).

Active-Site Mechanistic Crosslinking as a Method to Probe FabA Activity

Early studies of FabA utilized radioactive isotopes and required the reconstitution of multiple enzymes and cofactors followed by fatty acid extraction and radioactivity analysis, which was difficult and expensive (Kass, 1967; Helmkamp, 1968; Kass, 1968). *In vitro* mechanistic crosslinking provides a facile and reliable alternative method to directly measure FabA activity (Fig. 2)(Worthington, 2010; Ishikawa, 2013). Previous biochemical characterization of FabA revealed that the relative initial rates for α,β-decenoate formation is 6 and 10 times greater when the acyl chain is tethered to AcpP than as the acyl-*N*-acetylcysteamine (SNAC) thioester derivative and pantetheine derivative, respectively (Brock, 1967; Leesong, 1996). In order to test whether an active-site mechanistic crosslinking assay is a valid method to probe for FabA activity, FabA was pre-incubated with free probe **DH10** (not attached to AcpP) as well as **DH10** previously loaded onto AcpP. Covalent attachment of **DH10** and **DH10**-AcpP to FabA was monitored by electrospray ionization mass spectrometry (ESI-MS) and gel shift assay, respectively (Fig. S3). The results indicate that covalent attachment of **DH10** to FabA was accomplished 10 times faster when **DH10** was tethered to AcpP, consistent with the previous reconstitution studies that highlight the importance of FabA-AcpP protein-protein interactions in FabA catalytic efficiency (Brock, 1967).

To further support our hypothesis that the active-site mechanistic crosslinking assay is suitable for assessing FabA activity, we screened FabA against the four crosslinking probes **DH6, DH8, DH10**, and **DH10X** attached to AcpP (Fig. S3). FabA displayed the greatest activity towards probe **DH10**-AcpP, which mimics the putative FabA 3-hydroxydecanoyl-AcpP substrate (Fig. S3). The higher FabA activity towards the 10 carbon crosslinker and increase in enzyme efficiency in the presence of AcpP both demonstrate that active-site mechanistic crosslinking is a valid and efficient method to probe for FabA activity.

FabA “Positive Patch” is Important for AcpP Interaction

A universal “positive patch” important for AcpP interactions with partner proteins in FASII has long been proposed and studied (Parris, 2000; Zhang, 2000; Zhang, 2003; White, 2005; Cryle, 2008; Babu, 2010; Guy, 2011; Crosby, 2012). The AcpP=FabA complex structure provided the first molecular details of the “positive patch” residues that interact specifically with negatively charged acidic residues located between helices II and III of AcpP (Fig. 1 and 4). In FabA this “positive patch” is comprised of R132, R136, R137 and K161 (Fig. 4a) (Nguyen, 2014). Whereas R132, R136 and K161 form salt bridges with acidic residues on AcpP, FabA R137 anchors the AcpP to FabA by forming a hydrogen bond with the

phosphate of the PPT arm from the AcpP-tethered DH10 substrate (Fig. 4b). To test the importance of the FabA "positive patch" residues, the R132E, R136E, R137E and K161E mutants were generated. As expected, the reversal of the charges of the "positive patch" residues led to drastic decreases in crosslinking efficiencies resulting in less than 50% complex formation for all four mutants across all four probes. The mutation with the lowest reduction in crosslinking yield is R137E (Fig. 4b). The higher retention in activity of the R137E mutant demonstrates that disrupting the hydrogen bonding between FabA and the PPT arm is the least critical interaction for anchoring FabA to acyl-AcpP during β-hydroxyl-AcpP dehydration (Fig. 4). These results provide the first direct evidence for the important role that the "positive patch" residues play in AcpP and FabA interactions and serves as a model for characterization of "positive patches" in other FAS II proteins.

Engineering FabA for Specific Chain Length Dehydration

To gain insights into how FabA substrate specificity is conferred, the substrate pockets of the *apo*-FabA, *holo*-FabA and AcpP=FabA were structurally aligned (Fig. S5b). These structural alignments demonstrate that the residues that line the FabA substrate pocket are highly similar between the three structures, suggesting that FabA substrate specificity is defined by a rigid substrate pocket topology and not by structural rearrangement of residues within the pocket. Because the length of the FabA substrate pocket appears to be involved in determining the length of the acyl chains that can be accommodated, we hypothesize that truncation or expansion of the FabA pocket may drive FabA to productively bind acyl chains with different lengths (Fig 5 and S5).

In all three FabA structures, the substrate-binding pocket contains an 11 A long hydrophobic cavity, which is large enough to accommodate the preferred 10 carbon fatty acyl substrate (Fig. 5 and S5). This substrate tunnel is lined with hydrophobic residues L28, G91, F92, L94, G103, A105 and L164 and closed off by F21 (Fig. 5 and S5). The bulky F21 residue is shifted towards the substrate in both *holo*-FabA and AcpP=FabA to form hydrophobic interactions with the bound ten-carbon inhibitors (Leesong, 1996; Nguyen, 2014). To test the hypothesis that the length of the FabA substrate tunnel determines acyl chain specificity, smaller residues were mutated to phenylalanine to constrict the pocket (Fig. 5a); and larger residues were mutated to alanine or glycine to enlarge the pocket (Fig. 5c). The activities of these mutants were assessed using *in vitro* crosslinking assays with probes **DH6, DH8, DH10**, and **DH10X** (Fig. 5b and 5d). The results demonstrate significant alterations in substrate preferences between the WT FabA and FabA with mutations in the substrate pocket.

L28F, G91F, A103F and A105F mutants were generated to constrict the size of the FabA substrate pocket. All four mutations led to reduced activity for the longer chain length probes **DH8, DH10** and **DH10X**. Whereas WT FabA, G91F, G103F and A105F share comparable activities for probe **DH6**, L28F displays an increase in crosslinking yield with probe **DH6** (Fig. 5b). To provide a rationale for the observed altered substrate specificities, we generated FabA mutant models using the "Mutate and Autofit" function in Crystallographic Object-Oriented Toolkit (COOT) (Fig S5c) (Emsley, 2010). These models predict that FabA mutants contain substrate pockets that are either narrowed (L28F) or

truncated (G91F, G103F, and A105F) relative to the FabA WT substrate pocket. Based on the L28F model, narrowing of the pocket by the L28F mutation may result in increased hydrophobic and Van der Waals interactions with shorter chain fatty acids, such as probe **DH6**, resulting in the observed increased crosslinking efficiency. In comparison, FabA A105F, which by COOT modeling displays the most truncated substrate pocket, retains a 10–15% crosslinking efficiency with all four probes (Fig. 5b). These results suggest that the FabA A105F substrate pocket is not entirely blocked but merely narrowed. It is possible that localized protein dynamics still allow crosslinker binding even in the presence of the bulkier phenylalanine residue.

In contrast to FabA mutations that constrict the substrate pocket, the FabA L94A, L164A, F92A and F21G mutants were generated to enlarge the substrate pocket (Fig. 5c). All four mutants retained significant crosslinking activity with probes **DH6, DH8, DH10** and **DH10X**, with efficiencies of at least 50% or greater relative to WT FabA (Fig. 5d). These results demonstrate that widening the pocket has less drastic effects on substrate binding than substrate pocket constriction. Interestingly, relative to WT FabA, the F21G mutant displays greater crosslinking efficiency with probe **DH6** and comparable activity with probes **DH8, DH10** and **DH10X**. These results demonstrate that the crosslinking efficiency of F21G is not hampered by the decrease in hydrophobic interaction at the bottom of the substrate tunnel. COOT modeling of the F21G mutant suggests that the absence of the bulky side chain of F21 may extend the length of the substrate pocket by opening up the substrate tunnel to bulk solvent (Fig. S5c). When WT FabA and the F21G mutant were transformed into a FabA knockout strain, the saturated and unsaturated fatty acid profiles and chain length of products of the two *E. coli* variants displayed very little variation (Fig. S6b–c). This demonstrates that *in vitro* data for the F21G mutant also translates *in vivo*.

FabA Gate-Keeping Residues are Important for Substrate Specificity

Recent molecular dynamic simulation studies of butyrylcholinesterase and acetylcholinesterase demonstrate the novel roles that “gating residues” play in determining substrate specificity (Fang, 2011). To explore the possibility that a similar gating mechanism is also involved in selection of specific fatty acid chain lengths in FabA, we compared the three FabA pocket entrances in the three FabA structures discussed above. Comparison of the three structures revealed significant conformational changes at “gating residues” F165 and F171, the C-terminal residue, that define the entrance to the FabA active site tunnel (Fig. 6a–c). In the *apo* structure, these two residues close off the FabA pocket to the exterior solvent. In *holo*-FabA, F171 is repositioned to partially open the tunnel. In the AcpP=FabA structure, F165 is rotated and F171 is completely displaced from the entrance to the FabA active site tunnel. The structural rearrangements of the “gating residues” in the AcpP=FabA structure result in an active site tunnel entrance that is completely opened and accessible to the acyl-AcpP.

To evaluate the functions of F165 and F171, we generated their corresponding alanine mutants. *In vitro* crosslinking studies illustrate that alanine mutations of these “gating residues” result in a 3–4 fold increase in crosslinking efficiency with probe **DH6**, as compared to FabA WT (Fig. 6d). Both mutants, however, show only 50% crosslinking

efficiency relative to FabA WT with the longer probes **DH10** and **DH10X**. Overall, the F165A and F171A mutations resulted in similar crosslinking efficiencies for all four probes, **DH6, DH8, DH10**, and **DH10X** (Fig. 6d). These results suggest that mutation of the "gating residues" interferes with the ability of FabA to differentiate between different acyl-AcpP chain lengths and supports the hypothesis that the "gating residues" F165 and F171 serve as the initial selection filters for the incoming substrates. When WT FabA and the F171A mutant were transformed into a FabA knockout strain, the saturated fatty acid profile remained unchanged between the two transformed *E. coli* variants (data not shown.) The unsaturated fatty acid profile of the F171 mutant, however, shows a decrease in the common unsaturated fatty acids in *E. coli* (C16:1Δ9, C18:1 and cyclic C17:0), and the emergence of new unsaturated C16 fatty acids. These results demonstrate that the *in vitro* data for the F171A mutant translates to an *in vivo* setting as well (Fig. S6b–c).

We hypothesize that when AcpP approaches the FabA surface, the AcpP-tethered acyl chain interacts with and displaces F165 and F171 to allow substrate access to the FabA active site tunnel. Based on these new findings, it is likely that F165 and F171 serve as a hydrophobic surface to attract medium to long-chain fatty acids, thus offering a rationale for the observed low FabA affinity towards short-chain fatty acids. A sequence alignment of FabA and homologues (Fig. S4i) demonstrates that F165 and F171 are conserved in FabA from *E. coli* and *P. aeruginosa*, but not in the 5 FabZs that were analyzed. The "gating residue" in *H. pylori* FabZ was identified as Y100, where the mutant Y100A had a 50% decrease in enzyme activity (Zhang, 2008). This tyrosine residue is conserved in FabZ from *E. coli*, *P. aeruginosa*, *H. pylori*, *E. faecalis*, as well as the FabZ homolog FabN from *E. faecalis* (Lu, 2005). Because FabA and FabZ contain a substrate tunnel that are approximately equal in length (Kimber, 2004; Leesong, 1996), the difference in gating residues between the two enzymes may provide a mechanism for their different substrate preferences.

Conclusion

FabA β-hydroxyacyl-AcpP dehydration activity is dependent on productive interactions with specific chain lengths of acyl-AcpP (Leesong, 1996). In Nature, the preferred FabA substrates are medium chain length fatty acids centering around ten carbons (Heath, 1996). To provide insights into the FabA substrate selectivity and protein-protein interactions with AcpP during fatty acid dehydration, we generated fourteen structure-based FabA mutants and systematically tested their activities with 4 mechanistic crosslinking probes mimicking varying acyl chain lengths. The fourteen FabA mutations are classified into three defined FabA regions: the "positive patch," the substrate tunnel, and the "gating residues".

Crosslinking assays with the "positive patch" FabA mutants demonstrate that reversal of the positive charges leads to a large decrease in FabA activity, likely as the result of less productive interactions with AcpP. These results highlight the importance of the "positive patch" for proteinprotein interactions, and the importance of FabA-AcpP interactions for the activity of FabA. Out of the 8 FabA pocket mutants, with either a truncated or expanded substrate pocket, L28F appears to contain a substrate pocket that is most constricted. It is likely that the presence of the larger hydrophobic residue increases hydrophobic interactions with short-chain substrates, resulting in an increase in crosslinking efficiency towards **DH6**.

The FabA F21G model suggests that this mutant contains an expanded substrate pocket. The higher activity of the FabA F21G towards shorter probe **DH6**, retained activity for longer probes **DH10** and **DH10X**, and expanded pocket makes this mutant a possible means to produce both short and long chain fatty acids. The FabA "gating residue" mutants, F165A and F171A, displayed similar activities with all 4 probes, illustrating decreased ability to discriminate between varying acyl chain lengths. These results demonstrate that the "gating residues" act as the initial substrate selection filter, likely serving as a hydrophobic surface for medium-chain fatty acids.

Significance

These studies demonstrate that crosslinking can serve as a powerful tool to assess enzyme activity and the dynamic events between AcpP and FabA. Utilizing a panel of mechanistic crosslinking inhibitors in parallel with site-directed mutagenesis, we have gained insight into the complex interaction between AcpP and a partner protein. Importantly, this work marks the first alteration of FabA substrate specificity by a structure-based mutagenesis approach. We demonstrated that chain length specificity by FabA is determined not only by the substrate pocket, but also by surface "gating residues". To our knowledge, this is the first evidence demonstrating how "gating residues" influence fatty acid chain length production. Significantly, our work provides the framework for the engineered biosynthesis of both short and long chain fatty acids, which has applications for the production of biofuels. Additionally, we showed the first direct evidence of the importance of the partner protein "positive patch" for AcpP interaction, which can be important for the development of FAS II targeted antibiotics.

Methods

Probe Synthesis

Pantetheine analogues **DH6, DH8**, and **DH10** were synthesized from the assembly of three core scaffolds; a β,γ-unsaturated alcohol of varying length for the warhead portion, 3-chloropropylamine for the linker and p-methoxybenzyl-protected pantothenic acid to ultimately be converted into CoA and loaded onto the carrier protein. Pantetheine analogue **DH10X** was synthesized from 6-amino-1-hexanol rather than 3-chloropropylamine in order to extend the pantetheine portion of this probe. For full synthetic schemes, procedures, spectra and analysis see Supporting Information.

Site-directed Mutagenesis

The non-cleavable His_6-tagged FabA template was generously provided by Dr. Hirotada at Keio University, Japan. The FabA gene was cloned into the pET28b expression vector and used as the DNA template for site-directed mutagenesis with the mutagenic primer listed in Table S2. Polymerase chain reactions (PCR) were performed using a combination of varying DMSO and magnesium concentration and "step down" annealing temperatures. FabA PCR products were digested with Dpn1 to eliminate template WT FabA. Digested PCR products were transformed into NovaBlue (EMD Millipore). Single colonies were isolated and their

plasmids were extracted using Qiagen Minipreps. Site-directed mutagenesis was verified *via* DNA sequencing (IDT).

Protein Expression and Purification

The FabA and AcpP recombinant proteins were overexpressed in *E. coli* BL21 (DE3) (Novagen) *and E. coli* BL21 pLysS (DE3) (Novagen), respectively, and grown in LB. pET28b derived constructs were grown in the presence of 50 mg/L kanamycin and pET52b derived constructs were grown in the presence of 50 mg/L carbenicillin. Cells were induced with 1 mM IPTG at OD_{600} = 0.8 and aerated by shaking at 18 °C for 12–18 hours. The pelleted cells were re-suspended and lysed by sonication in 150 mM Tris-HCl (pH 7.5 at r.t.), 150 mM NaCl, and 20 % glycerol. The lysate was then spun at 14K RCF for 1.5 hours to remove insoluble debris. The His_6-tagged proteins were purified using Talon Metal Affinity Resins (ClonTech). The His_6-tags were cleaved with bovine thrombin (10 U per 1 mg protein) for 48 hours at 22 °C while dialyzing against 50 mM sodium phosphate (pH 8 for FabA and pH 7 for AcpP). To remove uncleaved proteins and thrombin, the protein-thrombin mixtures were re-purified using Talon Metal Affinity Resins (ClonTech) followed by a HiTrap Q anion exchange column with a gradient from 0 M to 1 M NaCl in 25 mM sodium phosphate (pH 8 for FabA and pH 7.0 for AcpP). FabA has a low affinity to the HiTrap Q (GE) column and elutes in the flow-through, while AcpP elutes at ~0.3 M NaCl. AcpP elution fractions containing impurities were collected, concentrated, and purified using Superdex200 (GE) gel filtration column. The FabA and AcpP were concentrated using Amicon Ultra Centrifugation Filters (Millipore) with 10 kDa and 3 kDa molecular weight cut off for FabA and AcpP, respectively.

Chemoenzymatic Loading and Purification

Apo-AcpP was prepared from a mixture of *apo*- and *holo*-AcpP according to a previous published protocol (Kosa, 2012). Final reaction concentrations: 50 mM potassium phosphate (pH 7.0), 4 mM ATP, 12.5 mM MgCl2, 0.01 μg/μL MBP-CoaA, 0.01 μg/μL MBP-CoaD, 0.01 μg/μL MBP-CoaE, 0.008 μg/μL Sfp (native), 0.6 μg/μL AcpP, 5% DMSO and 500 μM crosslinker probe. As a negative control, the crosslinker probe was replaced with equal volume of DMSO. After the addition of all components, reactions were gently mixed and incubated at 37 °C for 3 hours or overnight. The reaction mixture was centrifuged to remove precipitation, filtered using 0.45 μm syringe filter, and loaded on HiTrap Q anion exchange column to remove the coupling enzymes and unreacted crosslinking probes. The loaded AcpP eluted at ~0.3 M NaCl in 25 mM sodium phosphate (pH 8.0). The eluted protein was collected and concentrated using Amicon Ultra Centrifuge Filters (Millipore) with 3 kDa molecular weight cut off. Loading of **DH6, DH8, DH10**, and **DH10X** onto AcpP were monitored using MALDI-TOF (AB SCIEX TOF/TOF 5800), which has a 0.5% margin of error.

In vitro Mechanistic Crosslinking and Quantification

Equal molar of 100 μM of FabA and AcpP were incubated at 37°C. Time points were taken at 0, 10 min, 30 min, 1 hr, 2 hr, 4 hr and 8 hr. Reactions were stopped by the addition of 6× loading dye and boiled for 5 min. Proteins were loaded on 4–20% SDS PAGE gradient gels

(Biorad) and ran at 150 volts. The SDS PAGE gels were washed in boiling water and stained with Deville coomassie dye (Deville Scientific) and scanned using Odyssey (LI-COR Biosciences). Intensities of the protein bands were calculated using the ImageStudioLite (LI-COR Biosciences) software. All crosslinking efficiencies were calculated after 8 hours, which was the timepoint where **DH10**-AcpP and FabA WT reached "completion." Crosslinking efficiencies were calculated by taking the intensity of the crosslinked band and dividing it by the intensities of the crosslinked, FabA and AcpP bands combined. The crosslinking rates for FabA WT and all mutants with all four probes were calculated over the first hour and over 8 hours, and the relative intensities are comparable (Fig. S4a–h). Crosslinking yields in this manuscript, when done in duplicate, show an estimated error of 10%.

FabA Mutant Protein Models

The FabA mutant models were generated using COOT (Crystallographic Object- Oriented Toolkit) using the "Mutate and Autofit" function and overlaying the model with the electron density map of FabA in the AcpP=FabA structure. Final adjustments to the mutated residues were accomplished by visual inspections. The Ramachandran plots were then calculated to ensure appropriate amino acid configurations.

Structural Alignments and Calculated Distances

Protein-protein alignments were calculated using PymolX11Hyprid using the "Align" function. Measurements were performed using the "Measure" tool also performed in PymolX11Hyprid.

In vivo fatty acid analysis studies

FabA WT and FabA mutant F21G, L28F, F171A plasmids were transformed into *E. coli* FabA knockout strains MH121 and AS249, and grown in the presence of kanamycin, chloramphenicol and oleic acid. 50 mL LB cultures of each containing 50 mg/L kanamycin, 25 mg/L chloramphenicol and 1 mM IPTG were aerated by shaking at 37 °C for 12 hours. The pelleted cells were washed twice with sterile PBS buffer, resuspended in 1 mL 1M methanolic acid and incubated at 65°C for 30 minutes. The FAMEs were extracted with 1 mL hexanes and separated/analyzed by GCMS.

Supplementary Material

Refer to Web version on PubMed Central for supplementary material.

Acknowledgements

We wish to acknowledge funding from NIH GM100305 and GM095970. We thank Dr. John Greaves (UC Irvine), Dr. Beniam Berhane (UC Irvine) and Dr. Yongxuan Su (UC San Diego) for mass spectral analyses, and Dr. Anthony Mrse for assistance with acquiring NMR spectral data. We thank Dr. John Cronan (UIUC) for FabA knockout strains MH121 and AS249.

References

Babu M, Greenblatt JF, Emili A, Strynadka NC, Reithmeier RA, Moraes TF. Structure of a SLC26 anion transporter STAS domain in complex with acyl carrier protein: implication for E. coli YchM in fatty acid metabolism. Structure. 2010; 11(18):1450–1462. [PubMed: 21070944]

Brock D, Kass LR, Bloch K. P-hydroxydecanoyl dehydrase II: Mode of Action. J. Biol. Chem. 1967:4418–4431. [PubMed: 4863739]

Cronan JE. The chain-flipping mechanism of ACP (acyl carrier protein)-dependent enzymes appears universal. Biochem. J. 2014; 460:157–163. [PubMed: 24825445]

Crosby J, Crump MP. The structural role of the carrier protein—active controller or passive carrier. Nat Prod Rep. 2012; 29(10):1111–1137. [PubMed: 22930263]

Cryle MJ, Schlichting I. Structural insights into a P450 carrier protein complex reveal how specificity is achieved in P450(Biol) ACP complex. Proc. Natl. Acad. Sci. USA. 2008; 105(41):15696–15701. [PubMed: 18838690]

Emsley P, Lohkamp B, Scott W, Cowtan K. Features and development of Coot. Acta Crystallogra D. 2010; 66:486–501.

Fang L, Pan Y, Muzyka J, Zhan C. Active site gating and substrate specificity of butyrlcholinesterase and acetylcholinesterase: Insights from molecular dynamics simulations. J. Phys. Chem. B. 2011; 115(27):8797–8805. [PubMed: 21682268]

Feng Y, Cronan JE. Escherichia coli unsaturated fatty acid synthesis: complex transcription of the fabA gene and in vivo identification of the essential reaction catalyzed by FabB. J. Biol. Chem. 2009; 284:29526–29535. [PubMed: 19679654]

Guy JE, Whittle E, Moche M, Lengqvist J, Lindqvist Y, Shanklin J. Remote control of regioselectivity in acyl-acyl carrier protein-desaturases. Proc Natl Acad Sci USA. 2011; 108(40):16594–16599. [PubMed: 21930947]

Heath RJ, Rock CO. Roles of the FabA and FabB β-hydroxyacyl-acyl carrier protein dehydratases in *Escherichia coli* fatty acid biosynthesis. J. Biol. Chem. 1996; 271:22795.

Helmkamp G, Rando R, Brock H, Bloch K. β-hydroxydecanoyl thioetster dehydrase: specificity of substrates and acetylenic inhibitors. J. Biol. Chem. 1968; 243:3229–3231. [PubMed: 4872868]

Ishikawa F, Haushalter R, Lee DJ, Finzel K, Burkart MD. Sulfonyl 3-alkynyl pantetheinamides as mechanism-based crosslinkers of acyl carrier protein dehydratase. JACS. 2013; 135(24):8846–8849.

Janssen HJ, Steinbuchel A. Fatty acid synthesis in *Echerichia coli* and its applications towards the production of fatty acid biofuels. Biotechnology for Biofuels. 2013; 7:7. [PubMed: 24405789]

Kass L, Brock D, Bloch K. Beta hydrocydecanoyl dehydrase. J. Biol. Chem. 1967:4418–4431. [PubMed: 4863739]

Kass L. N-acetylcysteamine. Inhibition *in vivo* of β-hydroxydecanoyl thioester dehydrase. J. Biol. Chem. 1968; 243:3223–3228. [PubMed: 4968523]

Kimber MS, Martin F, Lu Y, Houston S, Vedadi M, Dharamsi A, Fiebig KM, Schmid M, Rock CO. The structure of (3R)-hydroxy-acyl carrier protein dehydratase (FabZ) from Pseudomonas aeruginosa. J. Biol. Chem. 2004; 279(50):52593–52602. [PubMed: 15371447]

Kosa NM, Haushalter RW, Smith AR, Burkart MS. Reversible labeling of native and fusion-protein motifs. Nature Methods. 2012; 9(10):981–984. [PubMed: 22983458]

Lee SY, Choi YJ. Microbial production of short-chain alkanes. Nature. 2013; 502:571–574. [PubMed: 24077097]

Leesong M, Henderson B, Gillig J, Schwab J, Smith J. Structure of a dehydratase-isomerase from the bacterial pathway for the biosynthesis of unsaturated fatty acids: two catalytic activities in one active site. Structure. 1996; 4(3):253–264. [PubMed: 8805534]

Lu YJ, White SW, Rock CO. Domain swapping between *Enterococcus faecalis* FabN and FabZ proteins localizes the structural determinants for isomerase activity. J. Biol. Chem. 2005; 280(34): 30342–30348. [PubMed: 15980063]

Magnuson K, Jackowski S, Rock CO, Cronan JE. Regulation of fatty acid biosynthesis in Echerichia coli. Microbio. Rev. 1993; 57:522–542.

Masoudi A, Raetz CR, Zhou P, Pemble CW. Chasing acyl carrier protein through a catalytic cycle of lipid A production. Nature. 2014; 505(7483):422–426. [PubMed: 24196711]

Nguyen C, et al. Trapping the dynamic acyl carrier protein in fatty acid biosynthesis. Nature. 2014; 505:427–431. [PubMed: 24362570]

Parris KD, Line L, Tam A, Mathew R, Hixon J, Stahl M, Fritz CC, Seehra J, Somers WS. Crystal structure of substrate binding to Bacillus subtilis holo-(acyl carrier protein) synthase reveal a novel trimeric arrangement of molecules resulting in three active sites. Structure. 2000; 8(8):883–895. [PubMed: 10997907]

Torella J, Ford TJ, Kim SN, Chen AM, Way JC, Silver PA. Tailored fatty acid synthesis via dynamic control of fatty acid elongation. Proc Natl Acad Sci USA. 2013; 110(28):11290–11295. [PubMed: 23798438]

White SW, Zheng J, Zhang YM, Rock CO. The structural biology of type II fatty acid biosynthesis. Annu. Rev. Biochem. 2005; 74:791–831. [PubMed: 15952903]

Worthington A, Burkart M. One-pot chemo-enzymatic synthesis of reporter-modified proteins. Org. Biomol. Chem. 2006; 4:44–46. [PubMed: 16357994]

Worthington A, Porter D, Burkart M. Mechanism-based crosslinking as a gauge for functional interaction of modular synthases. Org. Biomol. Chem. 2010; 8:1769–1772. [PubMed: 20449476]

Zhang L, Liu W, Hu T, Du L, Luo C, Chen K, Shen X, Jiang H. Structural basis for catalytic and inhibitory mechanisms of β-hydroxyacyl-acyl carrier protein dehydratase (FabZ). J. Biol. Chem. 2008; 283(9):5370–5379. [PubMed: 18093984]

Zhang YM, Rao MS, Heath RJ, Price AC, Olson AJ, Rock CO, White SW. Identification and analysis of the acyl carrier protein (ACP) docking site on β-ketoacyl-ACP synthase III. J. Biol. Chem. 2001; 276:8231–8238. [PubMed: 11078736]

Zhang YM, Wu B, Zheng J, Rock CO. Key residues responsible for acyl carrier protein and β-ketoacyl-acyl carrier protein reductase (FabG) interaction. J. Biol. Chem. 2003; 278:52935–52943. [PubMed: 14527946]

Highlights

- The application of mechanistic crosslinking to evaluate FabA specificity
- Mutagenesis utilized to identify important residues for FabA substrate preference
- First gain-of-function FabA mutant for shorter chain length fatty acids

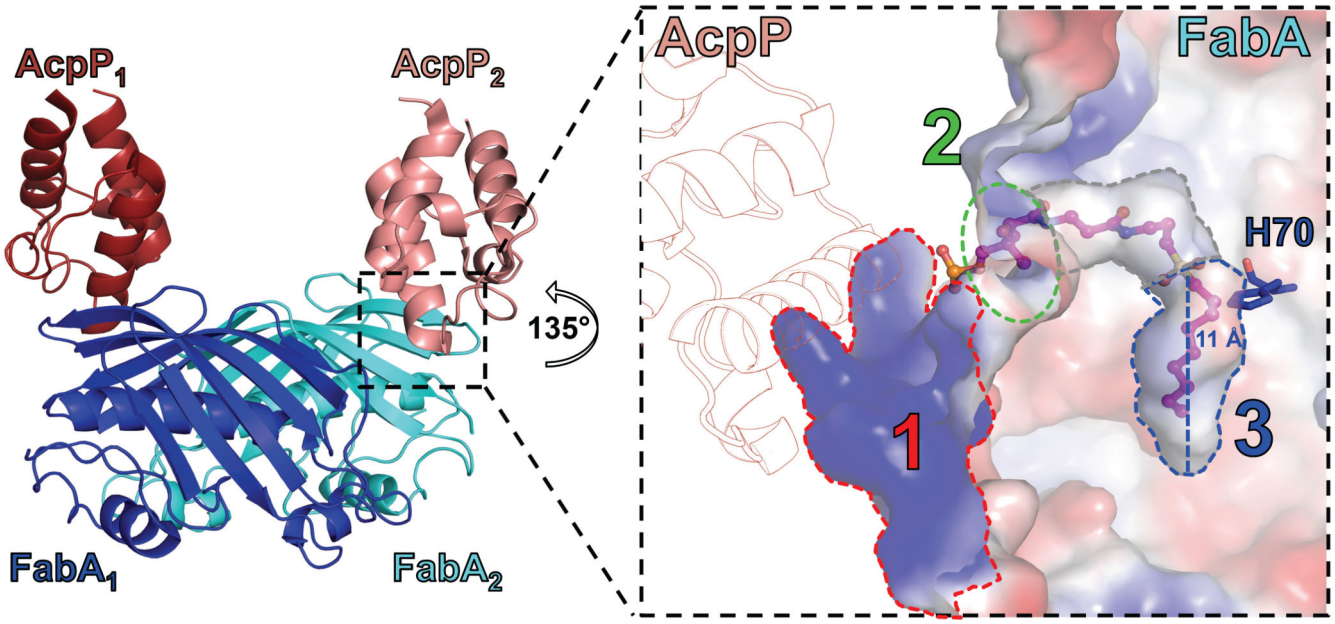

Figure 1. The three defined regions of FabA proposed to be important for substrate and acyl-AcpP interactions

The crosslinked structure of AcpP=FabA (PDB code: 4KEH) (left) and zoomed view of the FabA active site tunnel and AcpP interacting surface (right). The three defined FabA areas are (1) AcpP interacting surface is outlined in red dashes, (2) location of the “gating residue” is outlined in green dashes, and (3) substrate pocket is outlined in blue dashes. The length of the substrate pocket is in thin blue dashes. The PPT binding pocket is outlined in grey dashes. The bound **DH10** crosslinker is shown in magenta ball and stick. Active site H70 is shown in blue stick. FabA is shown in vacuum electro-static surface. AcpP is shown in salmon outline.

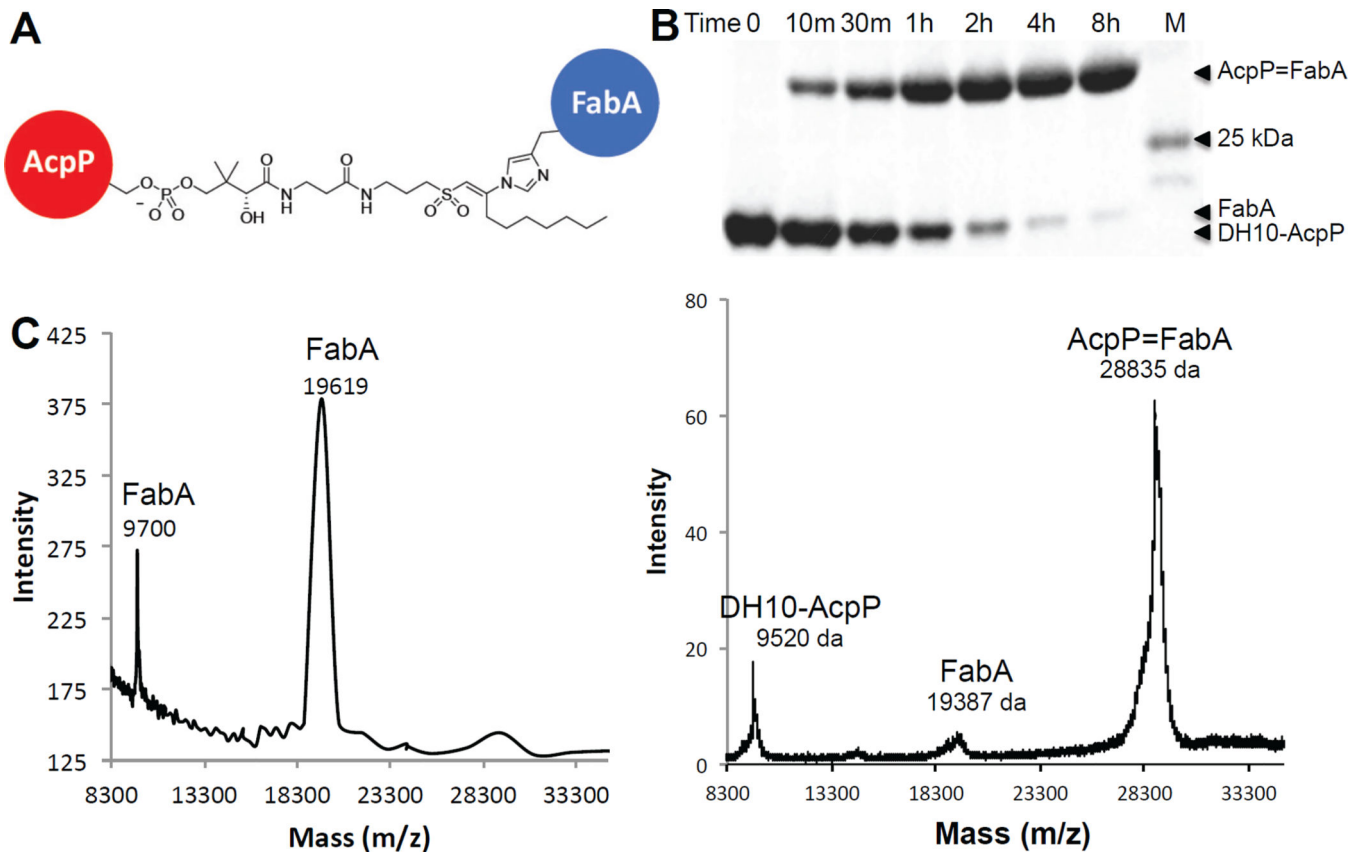

Figure 2. The FabA-AcpP mechanistic crosslinking assay

(a) The crosslinked complex of AcpP and FabA showing covalent attachment of the probe **DH10** to the catalytic residues H70 of FabA and S36 of AcpP. **(b)** SDS-PAGE analysis of **DH10**-AcpP FabA crosslinking. The AcpP-FabA complex formation is shown as a function of time, with >95% crosslinking yield after 8 hours. **(c)** MALDITOF MS spectra of FabA (left), expected mass of 19411 da and AcpP=FabA complex crosslinked with **DH10**-AcpP (right), expected mass of 28970 da.

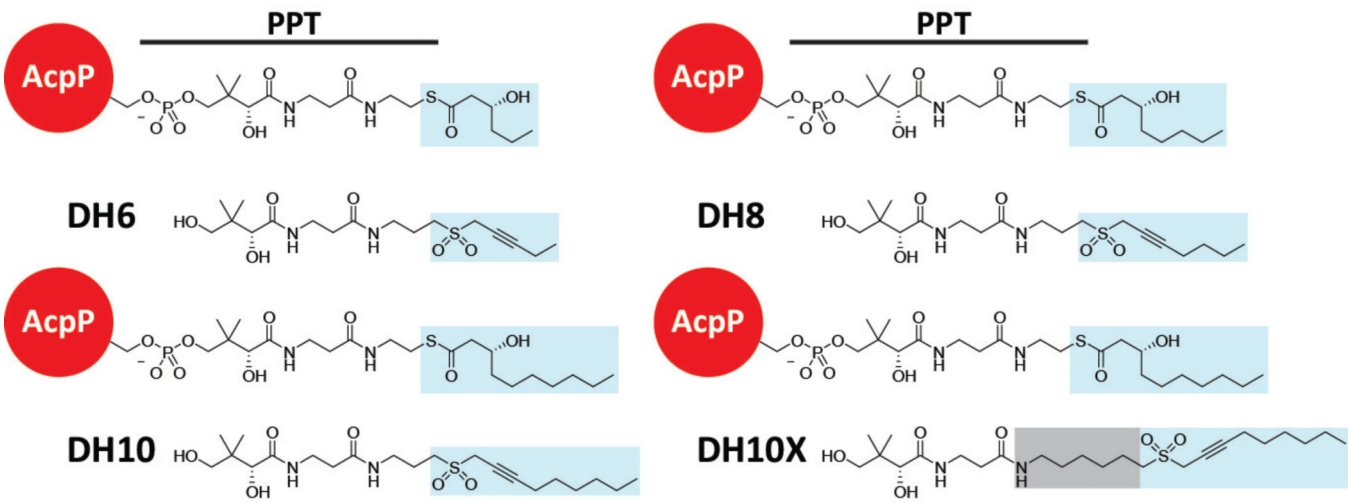

Figure 3. The FabA mechanistic crosslinking probes

The FabA mechanistic crosslinking probes **DH6, DH8, DH10**, and **DH10X** were synthesized with a sulfonyl-3-alkyne moiety to provide a site for covalent attachment of H70 of FabA. The four probes mimic the natural substrate, highlighted in blue, with an acyl group of C6 (**DH6**), C8 (**DH8**), C10 (**DH10**) and C10 with an extended phosphopantetheine portion (**DH10X**). The extended phosphopantetheine portion is highlighted in grey.

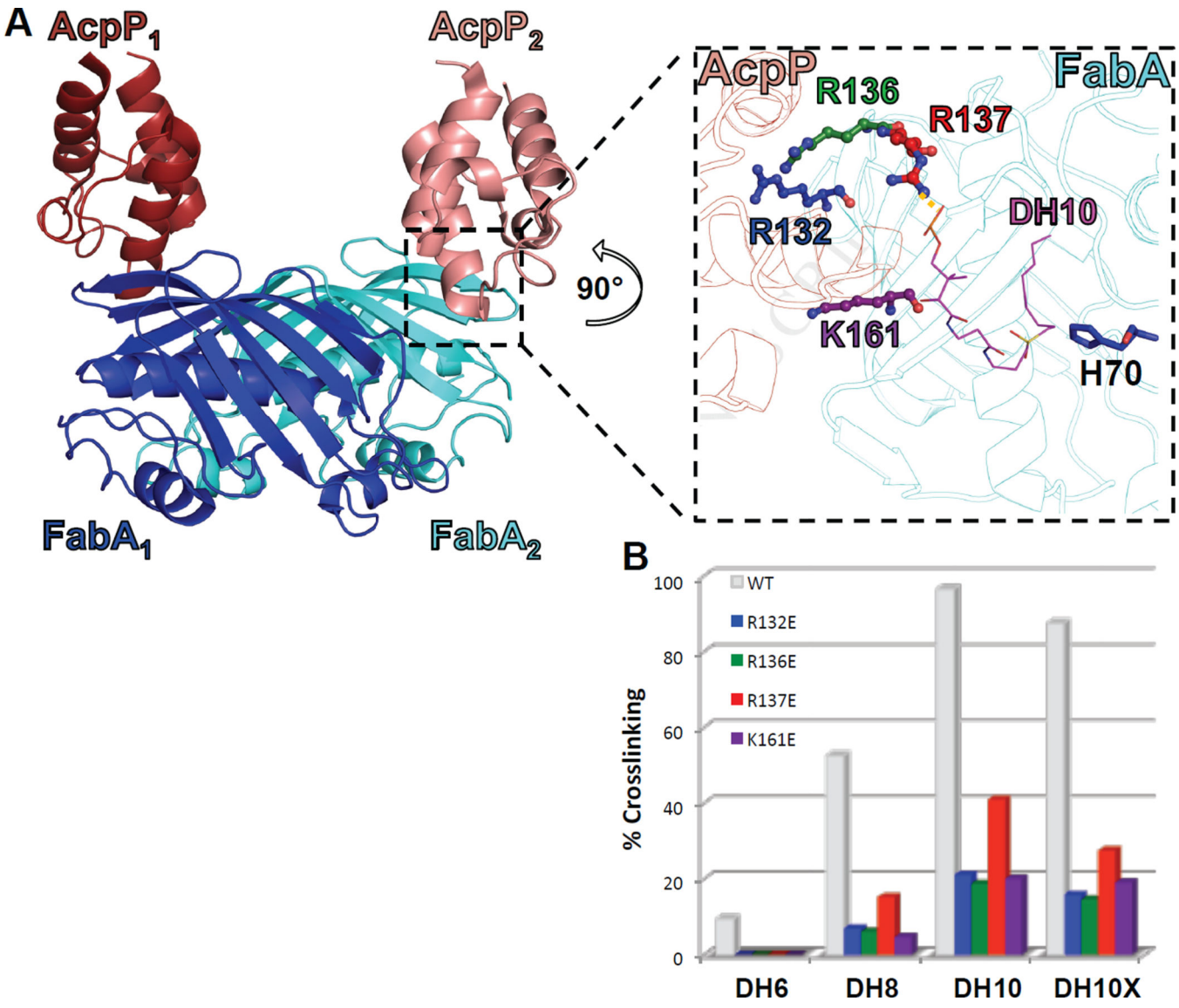

Figure 4. Mechanistic crosslinking assay with the FabA "positive patch" mutants

(a) The crosslinked structure of AcpP=FabA (PDB code: 4KEH) (left) and an expanded view of the FabA "positive patch," comprising of residues R132, R136, R137, and K161 shown in blue, green, red, and purple balls and sticks, respectively. The hydrogen bond between R137 and phosphate of the PPT group is shown in orange dots. The bound **DH10** probe is shown in magenta line. The active site H70 is shown in blue sticks. The FabA is shown as cyan outline and AcpP is shown in salmon outline. **(b)** *In vitro* mechanistic crosslinking assay of "positive patch" mutants with **DH6, DH8, DH10**, and **DH10X**, after 8 hours.

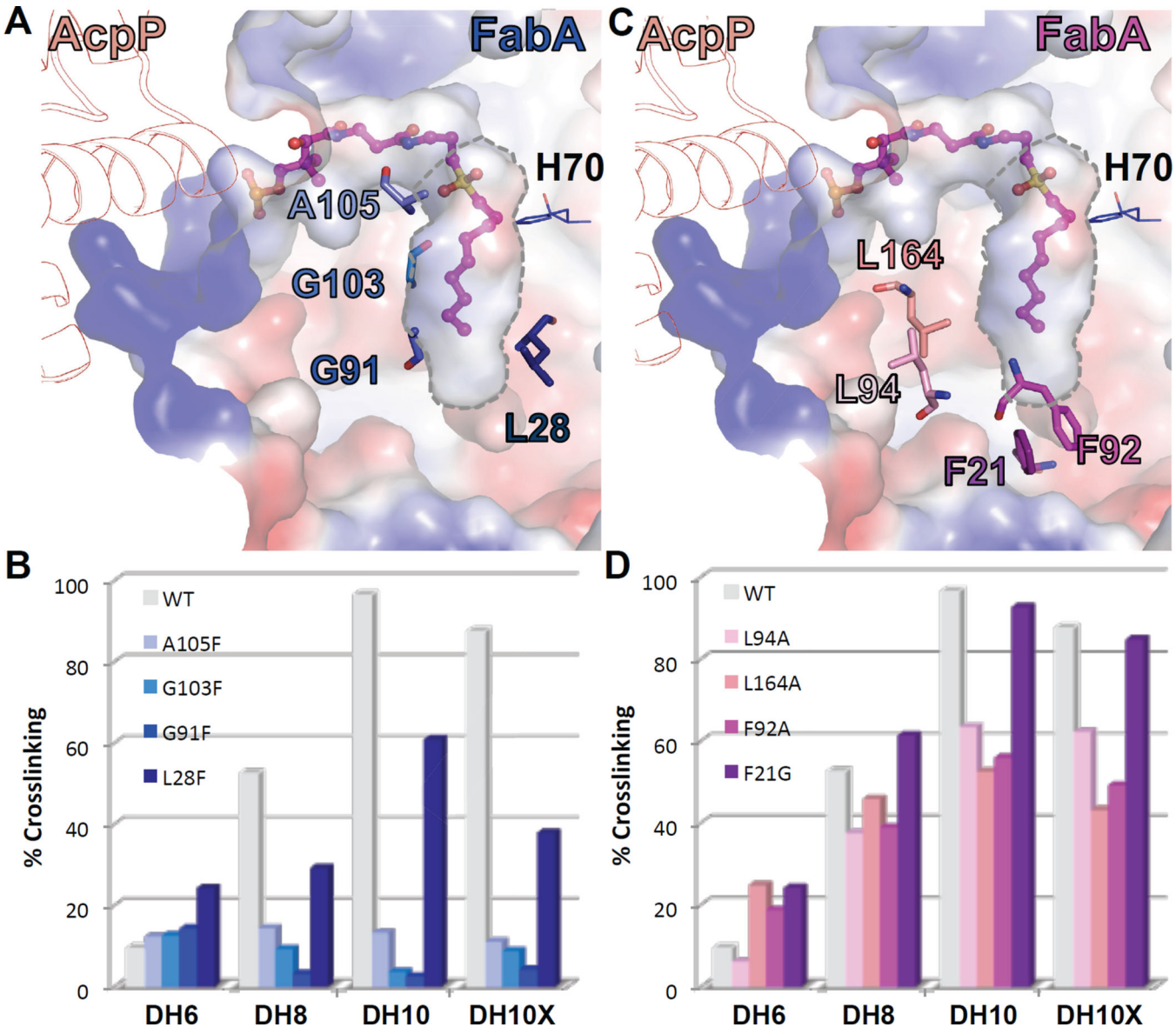

Figure 5. Mechanistic crosslinking assay with the FabA pocket residue mutants

(a) FabA residues that were mutated to truncate the FabA substrate pocket are shown in sticks with blue shading. Active site H70 is in blue lines. Bound **DH10** is in magenta ball and stick. The FabA surface is shown as vacuum electro-statics. AcpP outlined in salmon. **(b)** *In vitro* mechanistic crosslinking assay of FabA mutants A105F, G103F, G91F, and L28F with **DH6, DH8, DH10**, and **DH10X**, after 8 hours. **(c)** FabA residues that were mutated to expand the FabA substrate pocket are shown in sticks with pink shading. Active site H70 is in blue lines. Bound **DH10** is in magenta ball and stick. The FabA surface is shown as vacuum electro-statics. AcpP outlined in salmon. **(d)** *In vitro* mechanistic crosslinking assay of FabA mutants L94A, L164A, F92A, and F21G with **DH6, DH8, DH10**, and **DH10X**, after 8 hours

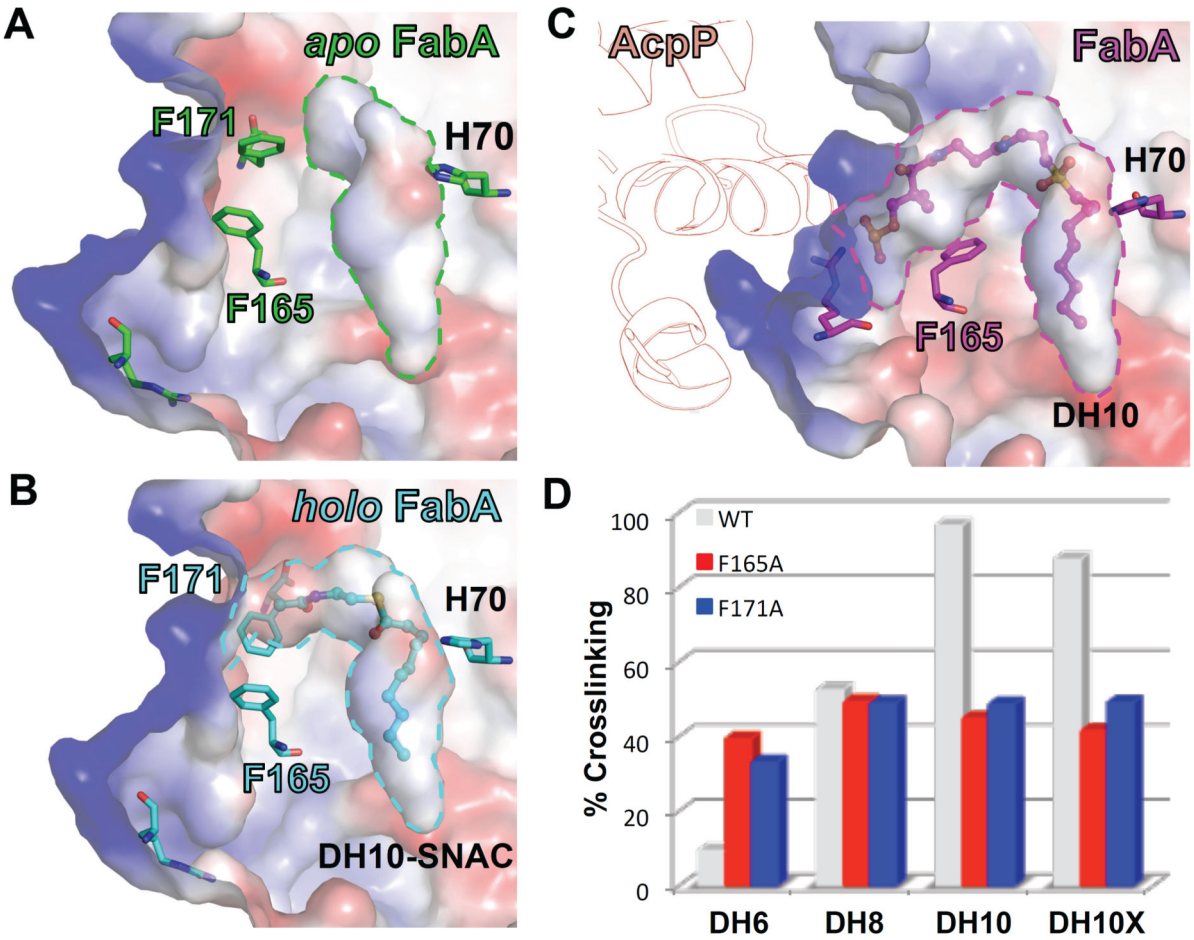

Figure 6. Mechanistic crosslinking assay with the FabA "gating residue" mutants

(a) The gating residues, F165 and F171 (shown as green sticks), in *apo*-FabA (PDB code: 1MKB) are positioned to completely block the FabA active site entrance. The active site H70 is shown in green stick and the *apo*-FabA structure is shown in vacuum electro-static surface. **(b)** In the *holo*-FabA structure (PDB code: 1MKA), F171 is rotated to partially open the FabA active site entrance. F165, F171, and active site H70 are shown in cyan sticks. The 3-decenoyl-SNAC is shown in cyan ball and stick. The *holo*-FabA structure is shown in vacuum electro-static surface. **(c)** In AcpP=FabA structure (PDB code: 4KEH), F165 is rotated and F171 is completely displaced to completely open the FabA active site entrance. F165, F171, and active site H70 are shown in magenta sticks. The **DH10** probe is shown in magenta ball and stick. FabA is shown in vacuum electro-static surface and AcpP in salmon outine **(d)**. *In vitro* mechanistic crosslinking activity assay of FabA "gating residue" mutants with **DH6, DH8, DH10**, and **DH10X**, after 8 hours.